Processing–Structure–Property Relationships in Poly(ethylene Terephthalate) Blown Film

TUNG CHAN MA and CHANG DAE HAN,* *Department of Chemical Engineering and Polymer Research Institute, Polytechnic University, Brooklyn, New York 11201*

Synopsis

An investigation was undertaken to establish processing–structure–property relationships in poly(ethylene terephthalate) (PET) blown film. For the study, a commercial grade of PET was used to fabricate the film specimens by means of a tubular film blowing process. In this process, the stretch temperature was accurately controlled by an oven. The annealing treatment of the oriented specimens involved clamping the sample in an aluminum frame and then putting the clamped sample in an oven, controlled at a temperature between the glass transition temperature (70°C) and the melting point (255°C) of PET, for a specified annealing period. The structure of the blown film samples was characterized by density, bulk birefringence, flat plate wide-angle X-ray scattering, and pole figure analysis. The processing variables, namely, takeup ratio, blowup ratio, and stretch temperature were found to significantly affect the bulk birefringence and density of the oriented PET blown film samples. It was found that both the bulk birefringence and density of the specimens increased upon annealing at an elevated temperature. Both the crystalline and amorphous orientation functions were calculated from the data of bulk birefringence, density, and the pole figure analysis. Compared to the amorphous orientation functions, the crystalline orientation functions were found to be relatively insensitive to the processing variables. It was concluded that equibiaxially oriented PET films can be produced via a tubular film blowing process by judiciously controlling the processing and annealing conditions. It has also been observed that the tensile stress-at-break of equibiaxially oriented PET film increases with decreasing stretch temperature and increasing annealing temperature.

INTRODUCTION

Poly(ethylene terephthalate) (PET) is a thermoplastic polyester, which is a condensation product of ethylene glycol and terephthalic acid. Due to the rigid benzene ring present in the PET chain, it has a glass transition temperature (T_g) of approximately 70°C and a melting point (T_m) of about 255°C, making it attractive to engineering applications. Films made from PET are considered to be hard and tough, and to have good dielectric properties, good electrical insulation properties, low gas and water vapor permeabilities, good transparency, and excellent gloss. PET films have many practical applications, such as in magnetic recording tapes, photographic films, capacitor layers, cable-wrapping insulating layers, and food packaging films.[1,2]

In the film blowing process, a polymer is extruded through an annular die to form a tubular bubble which is then quenched by an external cooling air stream distributed with the aid of a cooling ring. By expanding the tubular

*To whom all correspondence should be addressed.

Journal of Applied Polymer Science, Vol. 35, 1725–1757 (1988)
 CCC 0021-8995/88/071725-33$04.00

bubble with an inert gas between the die and nip rolls, biaxial orientation can be induced in the tubular bubble, as long as the takeup velocity of the nip rolls is greater than the linear velocity of the melt at the die exit.

The structure of biaxially stretched, semicrystalline polymer films can be characterized by studying: (1) the orientation distribution of the crystalline phase; (2) the orientation distribution of the amorphous phase; and (3) the degree of crystallinity. The overall orientation distribution of both crystalline and amorphous phases can be obtained by bulk birefringence measurements.[3] Wide-angle X-ray scattering (WAXS) can be used to determine the orientation distribution of the crystalline phase.[4] The degree of crystallinity can be calculated from density measurements.[5] The microstructure of oriented semicrystalline polymer films can be studied by other techniques, such as small-angle X-ray scattering (SAXS), small-angle light scattering (SALS), sonic modulus, infrared (IR) dichroism, fluorescence spectroscopy, Raman spectroscopy, nuclear magnetic resonance (NMR), and electron microscopy.[1-3,6,7]

The fluid mechanics aspects of the blown film process were first explored by Pearson and Petrie,[8] who simulated the isothermal blown film process, using a Newtonian fluid model. The nonisothermal blown film process was simulated by Han and Park[9] using a power-law fluid model, and by Haw and Han[10] using an integral-type rheological equation of state. Clegg and Huck[11] investigated the effects of various processing parameters on the physical/mechanical properties, and Clark and Garber[12] investigated the effect of processing variables on the morphology of polyethylene blown films. The development of crystalline orientation and the morphology of polyethylene blown films have been investigated by a number of research groups.[13-21] The orientation distributions of polypropylene blown films have been studied by others.[22-24] The development of crystalline orientation in polystyrene blown films was evaluated by Choi et al.[25] and Matsumoto et al.[26] To the best of our knowledge to date, the processing–structure–property relationships for PET blown films have not been reported.

The objectives of this study were: (1) to investigate the effects of processing variables on the degree of crystallinity and the mechanical properties of PET blown films; (2) to determine the effects of processing variables on the crystalline and amorphous orientation functions of the PET blown film; (3) to determine the effect of processing variables on the microstructure of the PET film produced.

BACKGROUND

Bulk birefringence (Δn) can be utilized to reveal the overall orientation in polymeric films.[3] Bulk birefringences are defined by the following expressions[3]:

$$\Delta n_{12} = n_1 - n_2 = -\Delta n_{21} \tag{1a}$$

$$\Delta n_{13} = n_1 - n_3 = -\Delta n_{31} \tag{1b}$$

$$\Delta n_{23} = n_2 - n_3 = -\Delta n_{32} \tag{1c}$$

where n_1, n_2, and n_3 are the refractive indices measured at 1-axis (machine

direction, MD), 2-axis (transverse direction, TD), and 3-axis (neutral direction, ND). Following the procedure due to Stein,[27] one can determine Δn_{12}, Δn_{13}, and Δn_{23} with a Babinet compensator.

The volume fraction of crystallinity (X) in a semicrystalline film sample can be calculated from the density of the specimen (ρ) by

$$X = (\rho - \rho_{am})/(\rho_c - \rho_{am}) \tag{2}$$

where ρ_{am} and ρ_c are the densities of the amorphous and the crystalline phases, respectively. Daubeny et al.[28] reported that the densities of the amorphous and crystalline phases of PET are 1.335 and 1.455 g/cm^3, respectively.

The orientation distribution of a crystallographic plane (hkl) with respect to the ith reference axis can be expressed in terms of the second moment of orientation, $\langle \cos^2 \chi_{i,hkl} \rangle$, which is defined by the following expression[29-31]

$$\langle \cos^2 \chi_{i,hkl} \rangle = \frac{\int_0^{\pi/2} I(\chi_{i,hkl}) \cos^2 \chi_{i,hkl} \sin \chi_{i,hkl} \, d\chi_{i,hkl}}{\int_0^{\pi/2} I(\chi_{i,hkl}) \sin \chi_{i,hkl} \, d\chi_{i,hkl}} \tag{3a}$$

where

$$I(\chi_{i,hkl}) = \int_0^{2\pi} I(\chi_{i,hkl}, \psi_{i,hkl}) \, d\psi_{i,hkl} \tag{3b}$$

and $I(\chi_{i,hkl} \; \psi_{i,hkl})$ is the X-ray scattering intensity distribution of (hkl) planes with respect to the ith reference axis in the spherical direction ($\chi_{i,hkl}, \psi_{i,hkl}$). The magnitude of $I(\chi_{i,hkl}, \psi_{i,hkl})$ can be determined from a pole figure analysis of the specimen.[4]

White and Spruiell[32] defined the crystalline orientation functions ($f_{i,j}$) of biaxially oriented specimens as follows:

$$f_{1,j} = 2\langle \cos^2 \chi_{1,j} \rangle + \langle \cos^2 \chi_{2,j} \rangle - 1 \tag{4a}$$

$$f_{2,j} = 2\langle \cos^2 \chi_{2,j} \rangle + \langle \cos^2 \chi_{1,j} \rangle - 1 \tag{4b}$$

where $\chi_{i,j}$ is the angle between the jth crystallographic axis and the ith reference axis. The following orthogonality relationship also exists for $\langle \cos^2 \chi_{i,j} \rangle$:[31,33]

$$\langle \cos^2 \chi_{1,j} \rangle + \langle \cos^2 \chi_{2,j} \rangle + \langle \cos^2 \chi_{3,j} \rangle = 1 \tag{5}$$

The state of orientation can be expressed by plotting $f_{1,j}$ vs. $f_{2,j}$, where all possible states of orientation for the jth crystallographic axis lie within an isosceles triangle as shown in Figure 1. In Figure 1, the origin represents the isotropic state while points X_1 and X_2 represent perfect uniaxial orientation along the 1- and 2-axes, respectively. Point X_3 represents polymer chains oriented perpendicular to the 1,2-plane. Points along the bisector of the angle $X_1X_3X_2$ represent the chains with equibiaxial orientation. Points along the

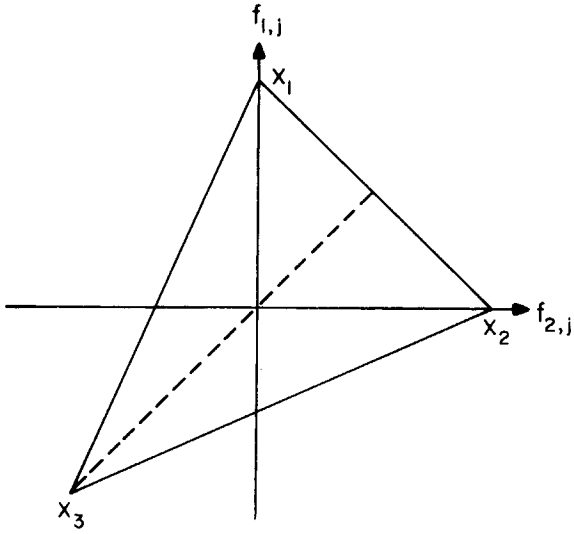

Fig. 1. The White–Spruiell orientation triangle plot.

base of the isosceles triangle (X_1X_2) represent the chains oriented parallel to the 1, 2-plane.

For biaxially oriented specimens, White and Spruiell[32] derived the following expressions which relate the bulk birefringences (Δn_{13} and Δn_{23}) to the volume fraction of the crystalline phase (X), the crystalline orientation functions ($f_{i,j}$), and amorphous orientation functions (f_i^{am}):

$$\Delta n_{13} = \left[X\left(f_{1,c}\Delta^{0cr}_{cb} + f_{1,a}\Delta^{0cr}_{ab}\right)\right] + \left[(1 - X)f_1^{am}\Delta^{0am}\right] + \Delta n_{13,\,form} \quad (6)$$

$$\Delta n_{23} = \left[X\left(f_{2,c}\Delta^{0cr}_{cb} + f_{2,a}\Delta^{0cr}_{ab}\right)\right] + \left[(1 - X)f_2^{am}\Delta^{0am}\right] + \Delta n_{23,\,form} \quad (7)$$

where $f_{i,c}$ and $f_{i,a}$ are the crystalline orientation functions of the crystallographic c- and a-axes, respectively, with respect to the ith reference axis, f_i^{am} is the amorphous orientation function of the chain axis with respect to the ith reference axis, Δ^{0cr}_{cb} and Δ^{0cr}_{ab} are the intrinsic birefringences of the cb and ab crystalline planes, respectively, of the unit cell, Δ^{0am} is the intrinsic birefringence of the amorphous phase, and $\Delta n_{13,\,form}$ and $\Delta n_{23,\,form}$ are the form birefringences of the 1, 3- and 2, 3-planes, respectively, of the specimen.

The first, second, and third terms on the right-hand side of both eqs. (6) and (7) represent the contributions of the crystalline phase, the amorphous phase, and the form birefringence, respectively, to the bulk birefringence. The form birefringence appears as a result of a distortion of the electric field at the anisotropically shaped phase boundaries.[3,34] The contribution of the form birefringence to the bulk birefringence is usually assumed to be negligible.[35] Since there is no independent method available which will allow us to directly determine the amorphous orientation functions (f_1^{am}, f_2^{am}), they can only be calculated indirectly from eqs. (6) and (7).

TABLE I
The Processing Conditions Employed for Sample Preparation

Sample no.	T_s (°C)	TUR	BUR
1	83	38.7	4.25
2	83	35.7	4.30
3	83	32.8	4.25
4	83	29.8	4.25
5	83	38.7	3.33
6	83	38.7	3.77
7	83	38.7	4.44
8	90	38.7	4.39
9	90	35.7	4.25
10	90	32.8	4.25
11	90	29.8	4.27
12	90	38.7	4.03
13	90	38.7	4.58
14	90	38.7	4.72

EXPERIMENTAL

Materials and Sample Preparation

A commercial grade of PET resin with an inherent viscosity of 1.06 was employed. In order to avoid hydrolytic degradation of PET at the extrusion temperature, PET pellets were dried in a vacuum oven at 150°C for 24 h, to minimize the moisture content before extrusion. Film specimens were fabricated by a film blowing process. In this process, the stretch temperature (T_s) was accurately controlled by an oven. Blown film specimens were collected at two values of T_s, specifically 83 and 90°C. The annealing treatment of the oriented specimens was carried out by clamping the sample in an aluminum frame and then placing the clamped sample in an oven, controlled at a temperature between the glass transition temperature (T_g), which is 70°C and melt point (T_m) which is 255°C, for a predetermined annealing period.

The annealed specimens were quenched in cold water to prevent further crystallization. For the ease of further discussion, let us define the following dimensionless parameters: blowup ratio (BUR) = A/a_0, and takeup ratio (TUR) = V/V_0, where a_0 is the outer radius of the annular die, A is the diameter of the tubular bubble leaving the oven, and V_0 and V are the linear speeds of the melt at the die exit and nip rolls, respectively. The processing conditions of the samples collected are listed in Table I.

Density Measurement

Film density was measured at 23°C by a density gradient column (Techne Inc., Model DC-1). A dense aqueous solution of calcium nitrate and water was used as the gradient forming fluid. For each sample, the density was measured at least five times and the average of the five measurements was used as the final value.

Birefringence Measurement

Birefringence measurements were made on an apparatus manufactured by Gaertner Science Corporation (Chicago). A mercury light source (GE H 100A 4/T), connected to a power supply (GE Gates Co., Model MLA-100), with a wavelength of 546 nm was employed. A Leitz Wetzlar goniometer, including a precision tilt angle adjustment device and two crystal hemispheres of refractive index $n_D = 1.516$, was used to mount and tilt film specimens. A Babinet compensator (Gaertner Model 447F) was employed to measure the optical retardation.

Wide-Angle X-Ray Scattering

Wide-angle X-ray scattering (WAXS) measurements were carried out for samples #1, #4, #5, and #7, and the pole figure analysis was performed for samples #1–7. The WAXS flat plate patterns were taken on a Statton

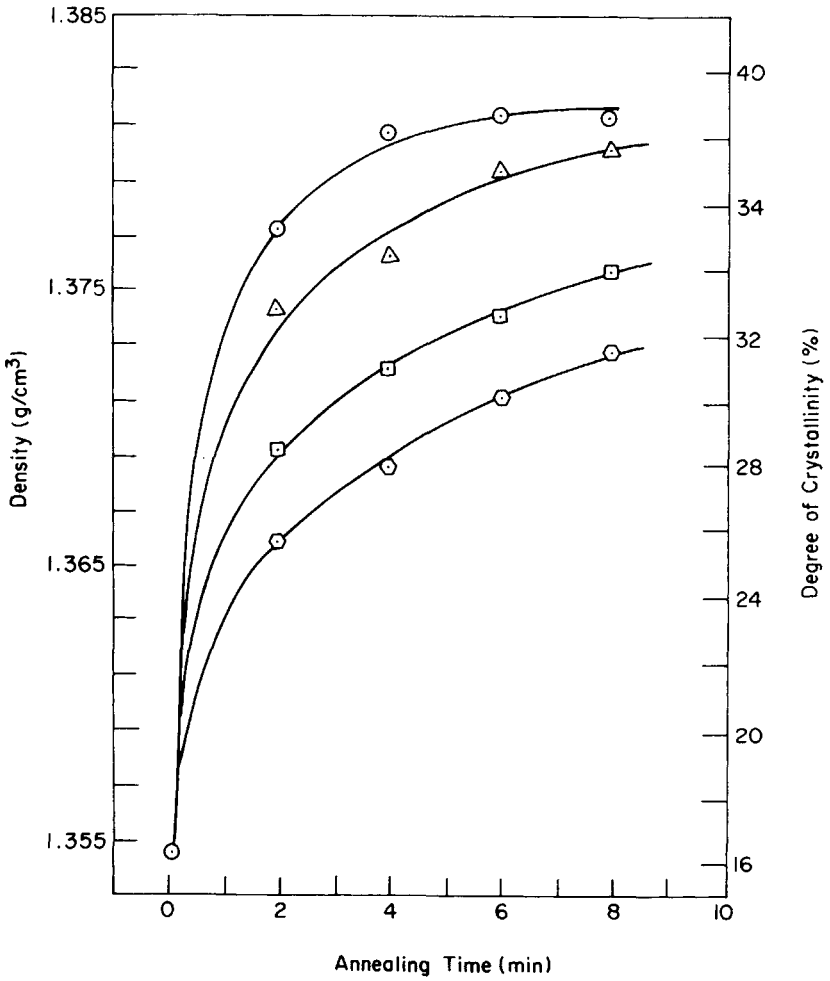

Fig. 2. The effect of annealing time on the density of samples stretched at 83°C, at different annealing temperatures (°C): (⊙) 200; (△) 190; (⊡) 170; (⊙) 150.

camera. X-rays were generated by a Phillips 4100 generator with a sealed tube, copper target (CuK_α), and nickel filter operating at 32 kV and 13 mA. Three WAXS flat plate pictures were taken for each sample with the incident X-ray beams directed in the machine direction (MD), transverse direction (TD), and normal direction (ND), respectively, of the sample. A sample-to-film distance of 3 cm was employed. Calcite powder was applied to the surface of the film stacks to calibrate the real sample-to-film distance, which was 2.80 cm.

The pole figure analysis was carried out on a single crystal orienter, equipped with a goniometer (General Electrical Co.). This device allows for the rotation of a stacked film specimen at a polar angle χ and an azimuthal angle ψ about two perpendicular axes. An IBM PC-XT with APEC (Akron Polymer Engineering Center) software was used to control the motion of the single crystal orienter and to analyze the collected data. X-rays were generated by a General Electric XRD-6 generator with copper target (CuK_α) and nickel filter operating at 40 kV and 20 mA. A scintillation counter (Bicron Corp., Model IXMP040B) was used to detect the intensity of the scattered X-ray beam. Pole figure data acquisition involved a step circular scan, in which a polar angle χ was set and azimuthal angle ψ increased from 0° to 360° at 10° increments. This process was repeated for different polar angles χ, in increments of 5°. After the backgrounds of the scattering peaks were determined and then subtracted, the intensities of the scattered X-rays were normalized to a scale ranging from 0.0 to 10.0 and plotted on a pole figure.

Tensile Properties Measurement

The tensile properties of the blown film samples were determined by an Instron testing machine (Model TM) at room temperature. For each sample, both the MD and TD tensile properties were measured. The average tensile properties of five specimens are reported here.

RESULTS AND DISCUSSION

Effects of Annealing on Density and the Degree of Crystallinity

The effects of annealing period and annealing temperature on the densities of the samples, stretched at 83°C, are shown in Figure 2. The density and the degree of crystallinity of the samples are seen to increase with annealing time and annealing temperature. During annealing, the oriented polymer chains acquire enough thermal energy to rearrange themselves in such a way as to minimize the structural defects formed during the stretching step. Thus, the packing efficiency of polymer chains is improved and the degree of crystallinity increased after annealing. The higher the annealing temperature (or the longer the annealing period), the more the thermal energy absorbed by the oriented polymer chains and the higher the degree of crystallinity of the specimens, as shown in Figure 2.

Determination of an Optimum Annealing Condition

The influence of annealing period on the tensile stress-at-break (σ_B) is given in Figure 3, where the σ_B in both MD and TD are observed to first increase

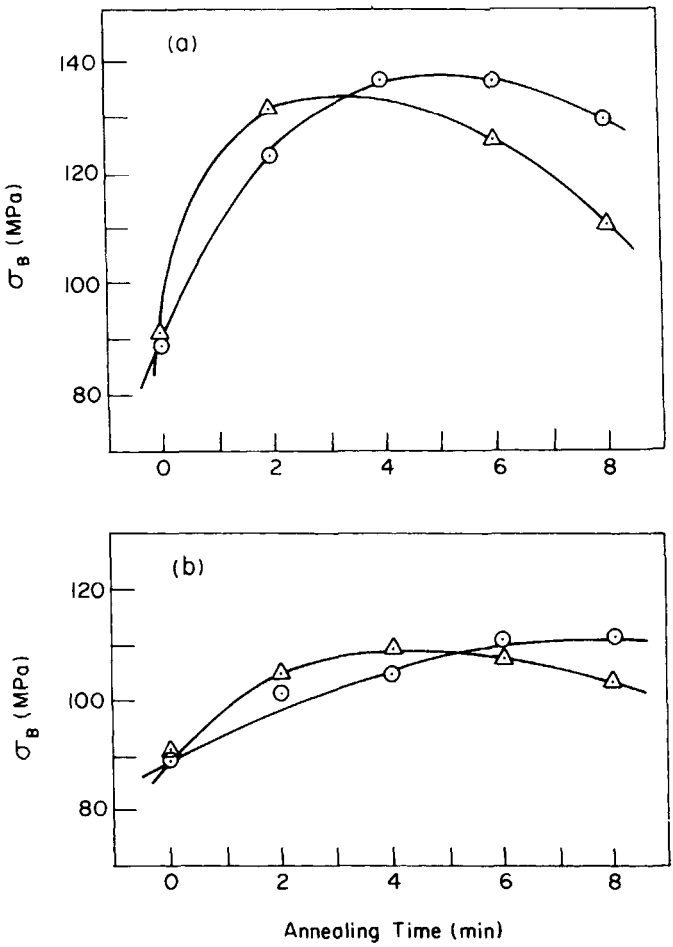

Fig. 3. The effect of annealing time on σ_B in the MD (⊙) and σ_B in the TD (△) for samples annealed at different temperatures (°C): (a) 200; (b) 170.

and then decrease with increasing annealing period. In the annealing step, the oriented PET specimens were heated up to a temperature between their T_g and T_m at fixed dimensions in an oven. At such an elevated temperature range, the oriented chains are able to rearrange themselves. As the annealing period increased, the degree of crystallinity increased, while the extent of chain orientation decreased due to the relaxation of the oriented chains. This may explain why σ_B goes through a maximum with annealing period.

As may be seen in Figure 3, the film samples annealed for a period of 220 s at 200°C were found to have the highest equibiaxial tensile stress-at-break, and therefore this particular annealing condition was considered to be an optimum for the oriented PET specimens produced in this study. Therefore, all the results reported below are based on this annealing condition, unless stated otherwise.

The effect of annealing temperature on σ_B for equibiaxially oriented film samples, stretched at 83°C, is given in Figure 4. The σ_B was seen to increase

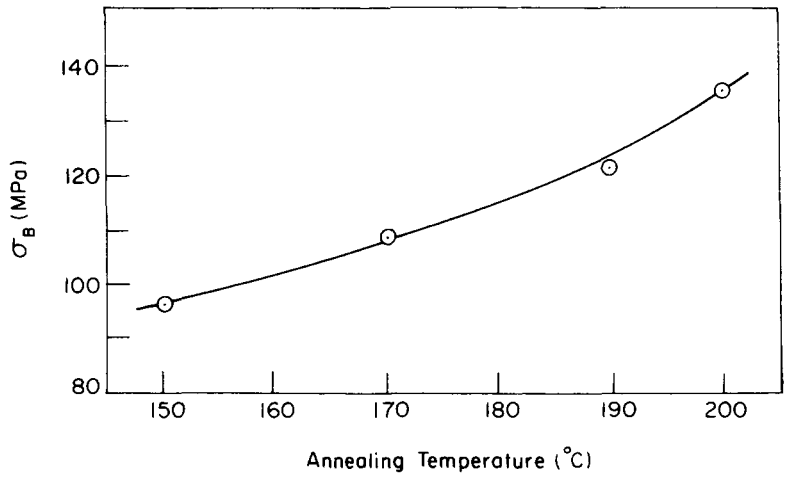

Fig. 4. The effect of annealing temperature on σ_B for equibiaxially oriented samples stretched at 83°C.

with annealing temperature, owing to the fact that structural perfection is improved with an increase in annealing temperature.

Effects of Processing Conditions on Bulk Birefringence

The dependence of bulk birefringences (Δn_{13}, Δn_{23}) on TUR for unannealed and annealed samples is shown in Figure 5. It can be seen in Figure 5 that Δn_{23} and Δn_{13} for the unannealed samples increase with TUR. It should be remembered that the bulk birefringence represents the overall orientation of the polymer chains in both crystalline and amorphous phases of the specimen.

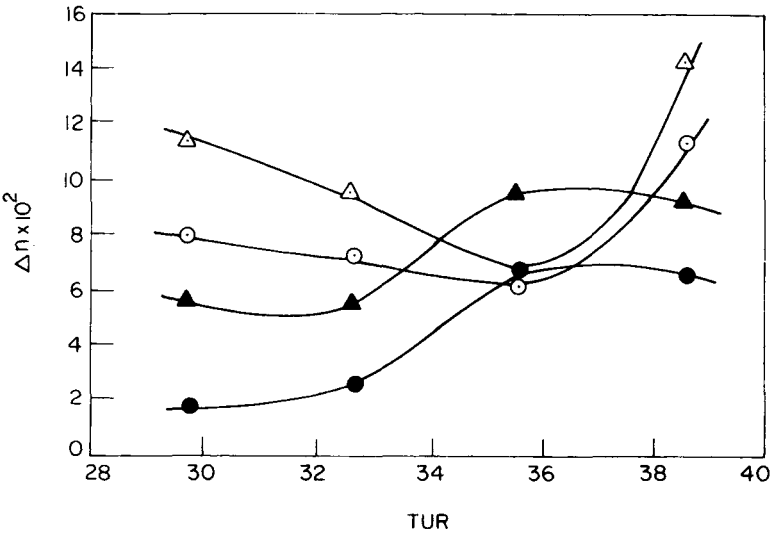

Fig. 5. The effect of TUR on birefringence at constant BUR 4.25 for samples stretched at 83°C. (a) Annealed samples: (⊙) Δn_{13}; (△) Δn_{23}; (b) unannealed samples: (●) Δn_{13}; (▲) Δn_{23}.

For annealed specimens, it can be seen in Figure 5 that Δn_{23} and Δn_{13} both go through a minimum with increasing TUR. Note that the annealed specimens have higher values of Δn_{23} and Δn_{13} than the unannealed ones, except between 33.4 and 37.3 TUR. Note that the polymer chains are rearranged during annealing and thus both the degree of crystallinity and structural perfection are improved. Therefore, during annealing, the overall orientation of macromolecules in the film sample is improved. This may now explain why the bulk birefringences of the annealed film samples are higher than the unannealed ones. However, the rearrangement of polymer chains during annealing can also cause a relaxation of the oriented polymer chains. This is the reason why the birefringence versus TUR relationship, given in Figure 5, for the annealed samples is so different from that for the unannealed ones.

The effects of BUR on Δn_{23} and Δn_{13} for the unannealed and annealed samples are given in Figure 6. It can be seen in Figure 6 that, for the unannealed samples, the birefringence first increases and then decreases with increasing BUR, going through a maximum. For the annealed samples, however, the opposite trend can be seen in Figure 6. Although the specimens were annealed at a fixed dimension by clamping the samples in an aluminum frame, a small percentage of film shrinkage might still have occurred. Film shrinkage induces molecular relaxation during annealing. Once a molecular relaxation occurs, the orientation of polymer chains is affected. This consideration may explain the reverse trend observed of the dependence of birefringence on BUR between the annealed and unannealed film samples.

Earlier, Devries et al.[37] reported that the birefringence in the plane of biaxially oriented PET film increased with increasing difference between the stretch ratio in two stretch directions, specifically, MD and TD. Jabarin[38] also reported that the birefringence of biaxially oriented PET sheets increased with decreasing stretch temperature (T_s) and increasing stretch ratio, while

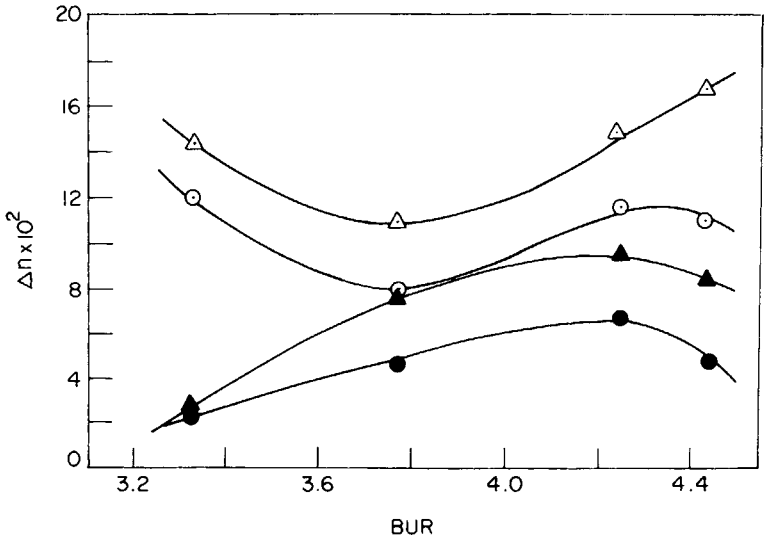

Fig. 6. The effect of BUR on birefringence at constant TUR of 38.7 for samples stretched at 83°C. (a) Annealed samples: (⊙) Δn_{13}; (△) Δn_{23}; (b) unannealed samples: (●) Δn_{13}; (▲) Δn_{23}.

Cakmak et al.[39] noted that the birefringence of biaxially oriented PET bottle increased with increasing inflation pressure.

Yokouchi et al.[40] reported that the birefringence of PET sheets, which had initially been stretched uniaxially at 80°C, increased with increasing stretch ratio. Biangardi and Zachmann[41] noted that an improvement in the mechanical properties of PET film was obtained by an increase in birefringence and by increasing the number of taut tie molecules. Zachmann[42] also reported that for uniaxially oriented PET sheets, the orientation of the amorphous phase

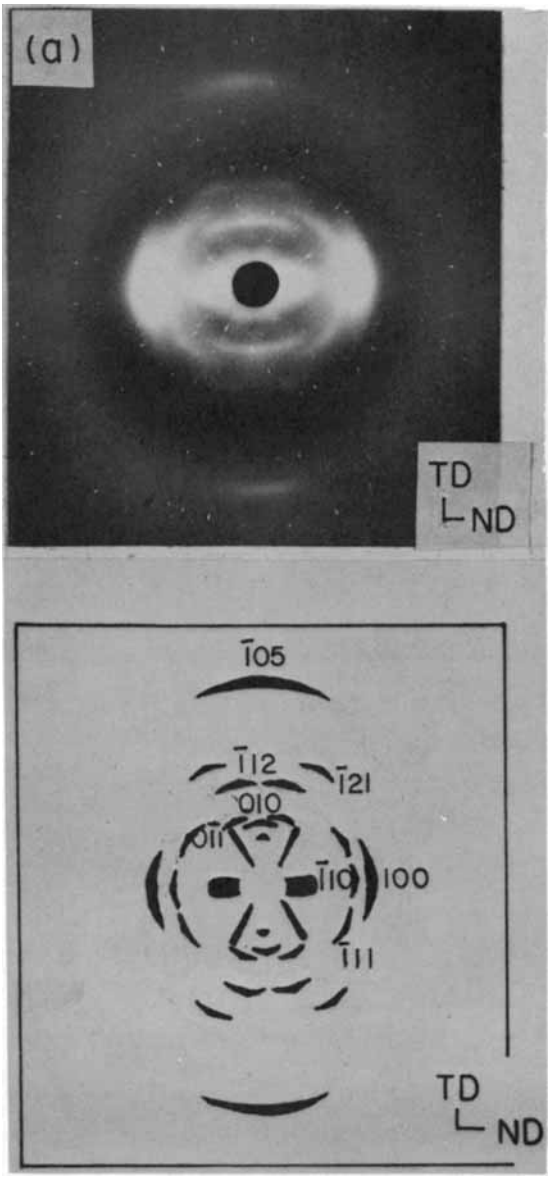

Fig. 7. The flat plate WAXS patterns of sample #1 taken with incident X-ray beam directed parallel to different directions: (a) MD; (b) TD; (c) ND.

increased with increasing film birefringence. He pointed out further that the fraction of the amorphous taut tie molecules decreased with increasing annealing temperature and with decreasing film birefringence.

Effects of Processing Conditions on WAXS Flat Plate Patterns

Daubeny et al.[28] identified PET as having a triclinic unit cell structure with lattice constants: $a = 4.56$ Å, $b = 5.94$ Å, $c = 10.75$ Å, $\alpha = 98.5°$, $\beta = 118°$, $\gamma = 112°$. Yoshihara et al.[43] proposed a pseudo-orthorhombic unit cell structure for PET with a'-, b'-, and c-axes specified. The direction perpendicular to

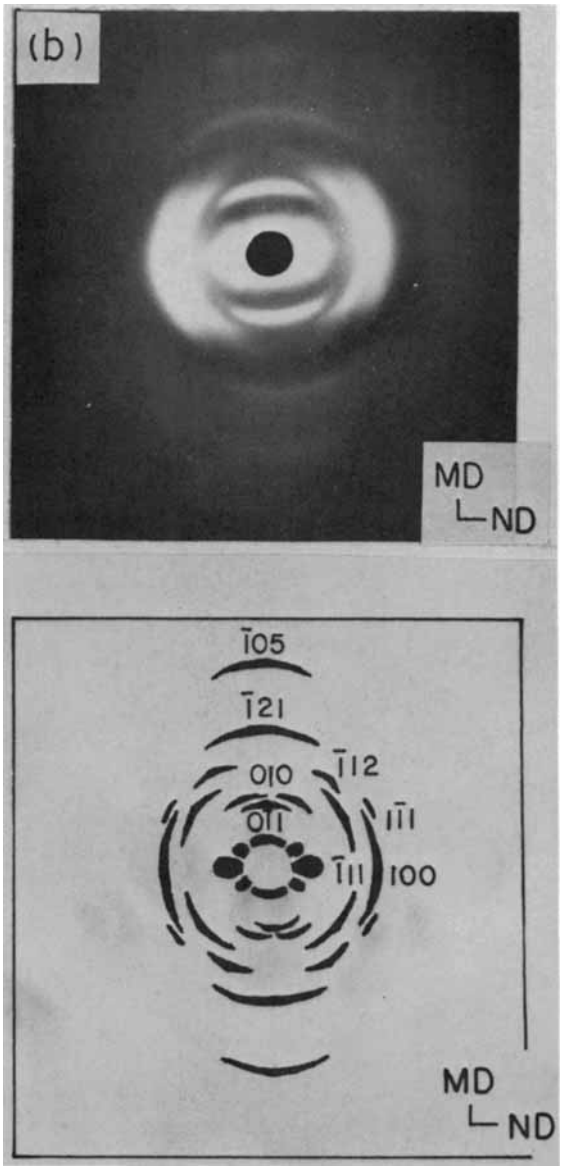

Fig. 7. *(Continued from the previous page.)*

the benzene ring plane in the PET chain is specified as the a'-axis. A third direction orthogonal to the a'- and c-axes is specified as the b'-axis.

On our WAXS flat plate patterns, 10 reflecting planes of the Debye-Scherrer rings were identified. In order of increasing interplanar spacing, they are: $(\bar{1}05)$, $(\bar{1}21)$, $(1\bar{1}1,)$ (100), $(\bar{1}12)$, $(\bar{1}10)$, $(\bar{1}11)$, (010), $(0\bar{1}1)$, and (001). From an analysis of the WAXS patterns, the following information was obtained[44]: (1) the $(\bar{1}05)$ plane normal makes an angle of 9.77° with the c-axis; (2) the benzene ring plane in the PET chain makes an angle of 18.84° with the (100) plane; and (3) the (010) plane normal makes angles of 80.23° and 59.44° with the $(\bar{1}05)$ and (100) plane normals, respectively. Hence, the orientation distri-

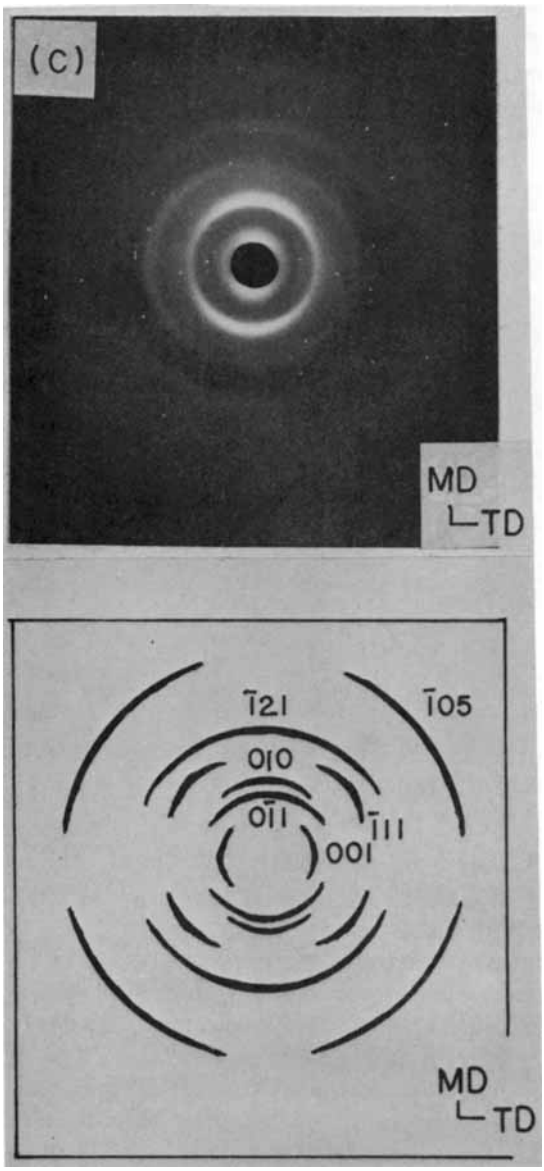

Fig. 7. (*Continued from the previous page.*)

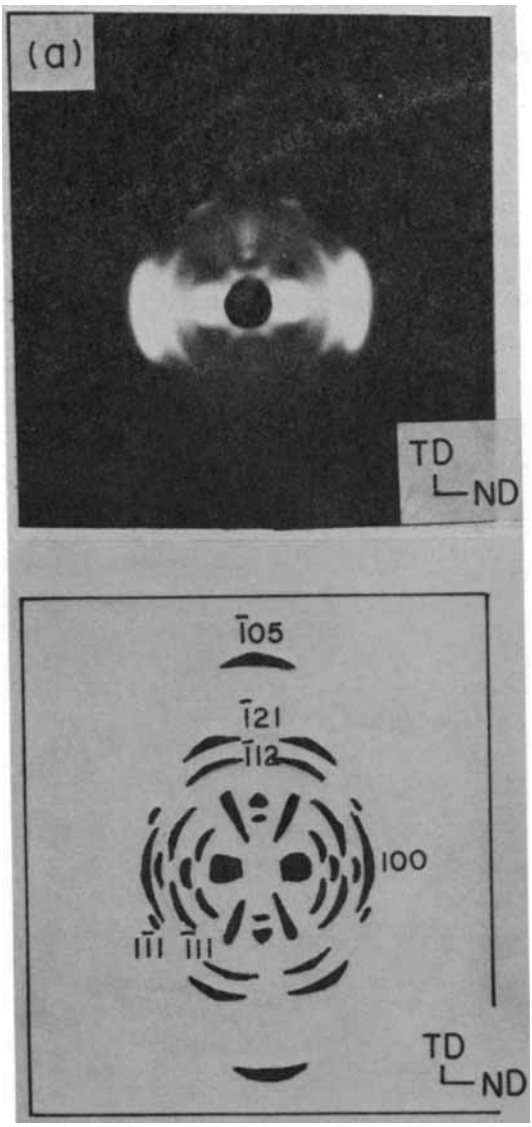

Fig. 8. The flat plate WAXS patterns of sample #4 taken with incident X-ray beam directed parallel to different directions: (a) MD; (b) TD; (c) ND.

butions of the c-, a'-, and b'-axes can be indicated by the pole figures of the ($\bar{1}05$), (100), and (010) planes, respectively.

The WAXS flat plate patterns for samples #1 and #4 are given in Figures 7 and 8, respectively. Since some of the X-ray reflections in the photographs did not give good contrast, they were traced and presented together with the photographs, in order to facilitate our discussion. Note, however, that the traced patterns only represent the shapes and positions of the X-ray reflections. The relative intensities of the X-ray reflections are better indicated in the photographs than in the traced patterns. Samples #1 and #4 have the same BUR 4.25, but the TUR of sample #1 is higher than that of sample #4

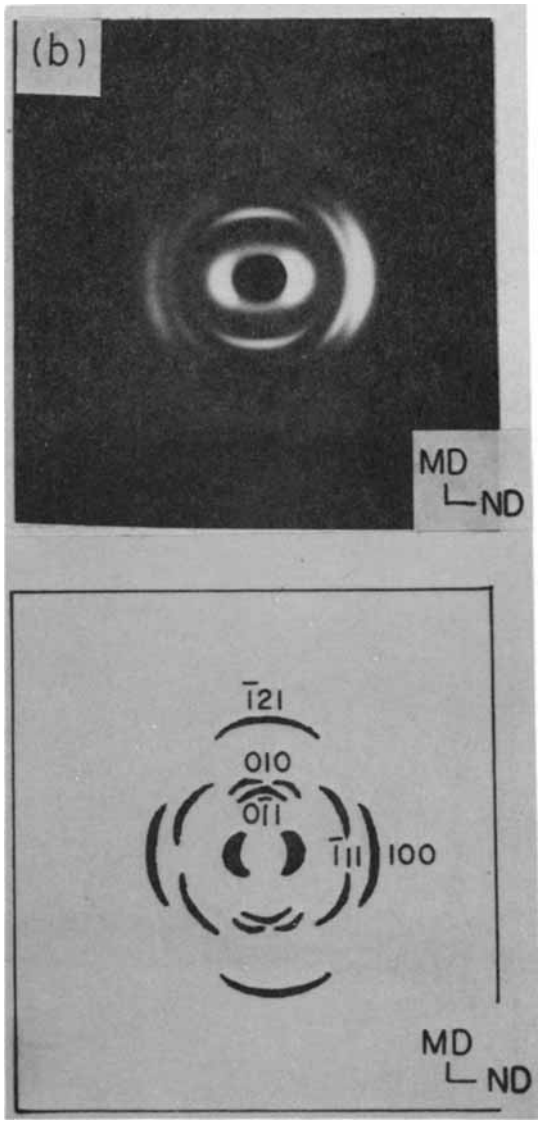

Fig. 8. (*Continued from the previous page.*)

(see Table I). The following observations may be made from Figures 7 and 8: (1) The intensities of the (001) reflection are stronger in sample #4 than in sample #1, meaning that the (001) plane normal is oriented closer toward the TD with decreasing TUR; (2) the $(0\bar{1}1)$ reflection plane in sample #4 [see Fig. 8(c)] forms an angle 20° with the meridian and its scattering intensity is much stronger than the scattering intensity in sample #1 [see Fig. 7(c)]; (3) a weak and diffuse $(0\bar{1}1)$ reflection in sample #1 [see Fig. 7(a)] is located on the meridian, but the $(0\bar{1}1)$ reflection in sample #4 [see Fig. 8(a)] is located at an angle 34° off the equator, meaning that the $(0\bar{1}1)$ plane normal is oriented closer toward the MD with decreasing TUR; (4) the intensity of the $(\bar{1}10)$ reflection in sample #4 [see Fig. 8(a)] is stronger than that in sample #1 [see

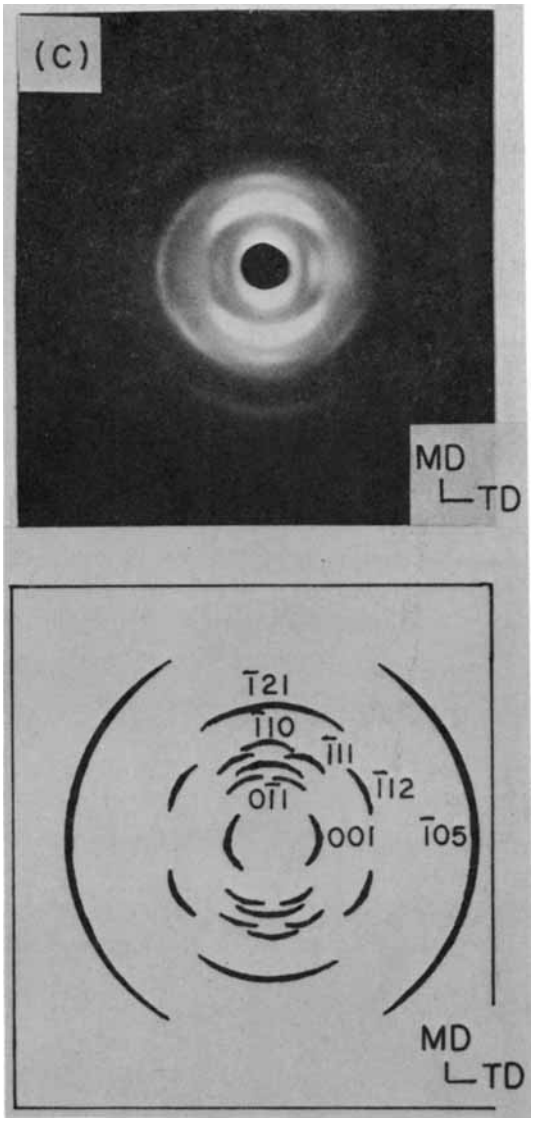

Fig. 8. (*Continued from the previous page.*)

Fig. 7(a)], meaning that the ($\bar{1}10$) plane normal is oriented closer toward the ND with decreasing TUR; (5) the orientation of the (100) plane is the same in both samples, meaning that the benzene ring planes in these two samples are oriented in a direction that is parallel to the film surface; (6) the ($\bar{1}05$) reflection plane in sample #4 is located on the meridian [see Fig. 8(a)] and its intensity is stronger than the intensity in sample #1 [see Fig. 7(a)]. We can conclude from the above observations that the PET chains in the two blown film samples are oriented closer toward the MD with increasing TUR.

The WAXS flat plate patterns for samples #5 and #7 are given in Figures 9 and 10, respectively. Note that the TUR of samples #5 and #7 are the same, but the BUR of sample #5 is smaller than that of sample #7 (see

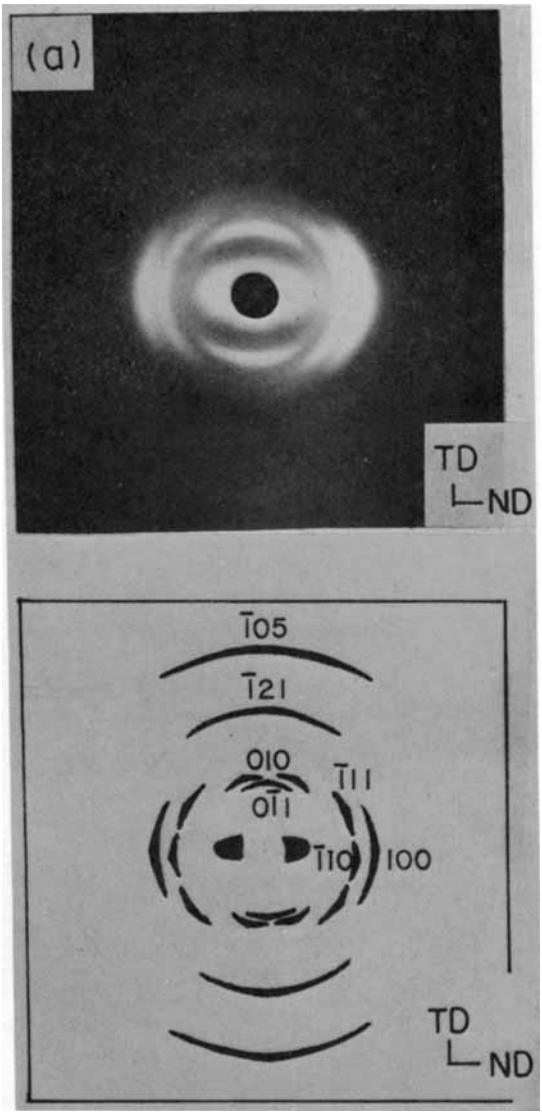

Fig. 9. The flate plate WAXS patterns of sample #5 taken with incident X-ray beam directed parallel to different directions: (a) MD; (b) TD; (c) ND.

Table I). The following observations may be made from Figures 9 and 10: (1) A very weak (001) reflection is located on the meridian in sample #5 (see Figure 9(c)), whereas it is on the equator in sample #7 [see Fig. 10(c)], meaning that the (001) plane normal is oriented closer toward the TD with increasing BUR. (2) The $(0\bar{1}1)$ and (010) reflections in sample #5 form concentric circles [see Fig. 9(c)]. On the other hand, the $(0\bar{1}1)$ and (010) reflections in sample #7 are located on the meridian and distributed towards the equator with decreasing intensity [see Fig. 10(c)]. Therefore, it can be concluded that the $(0\bar{1}1)$ and (010) plane normals are oriented closer toward the MD with increasing BUR. (3) The $(\bar{1}10)$ reflections in both samples are

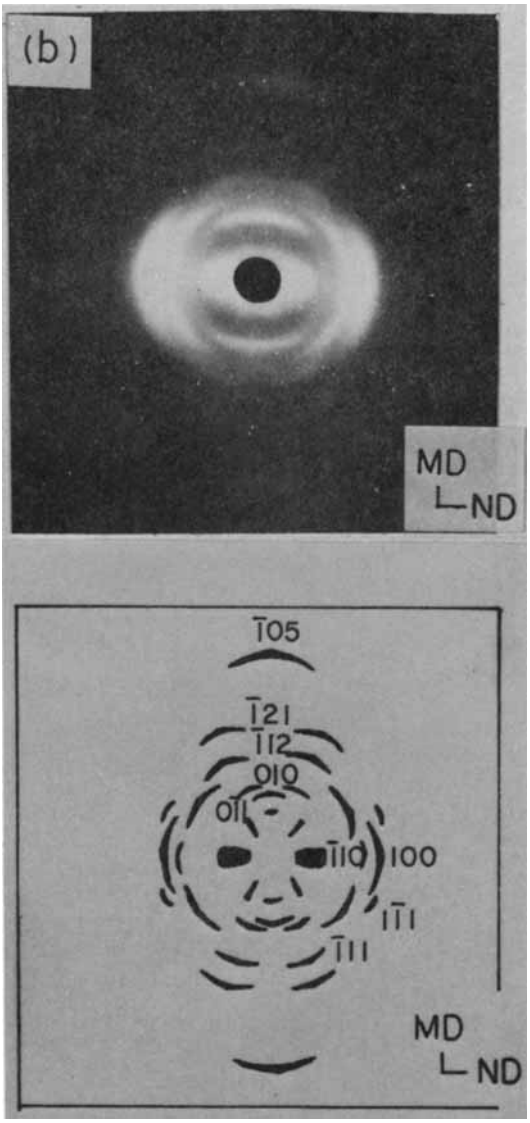

Fig. 9. (*Continued from the previous page.*)

located on the equators [see Figs. 9(a) and 10(a)], but the intensities are stronger in sample #7 than in sample #5, indicating that the ($\bar{1}10$) plane normal is oriented closer toward the ND with increasing BUR. (4) The (100) reflections in both samples are located on the equator with strong scattering intensities [see Figs. 9(a), 9(b), 10(a), and 10(b)], indicating that the planes of the benzene rings in the PET film are aligned parallel to the film surface. (5) In sample #5, the ($\bar{1}05$) reflections are located on the meridian, but the scattering intensities are much stronger in Figure 9(b) than in Figure 9(a), indicating that the chain axis is oriented nearly parallel to the MD of the film. (6) In sample #7, the ($\bar{1}05$) reflections are located on the meridian, but the scattering intensities are stronger in Figure 10(a) than in Figure 10(b), indicating that the chain axis is oriented toward a direction that is between MD and

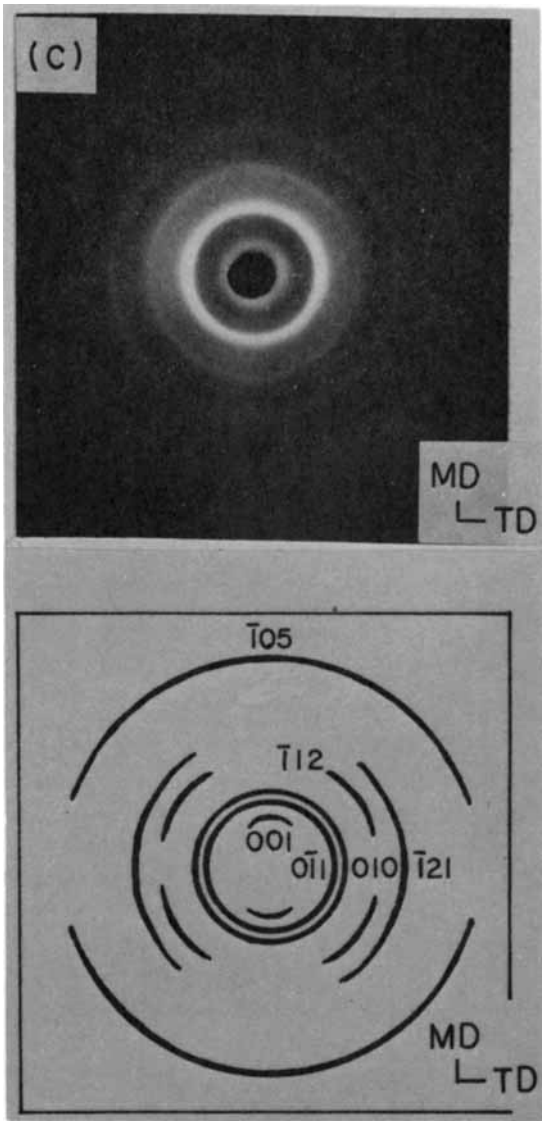

Fig. 9. (*Continued from the previous page.*)

TD, though more toward the TD than MD. We can conclude from the above observations that the chain axis in both films is oriented toward the TD with increasing BUR.

At this juncture, some of the earlier studies are worth noting. Dulmage and Geddes[45] examined the orientation distribution of amorphous PET film samples, stretched uniaxially at 90°C and annealed at 180°C. They concluded that the chain axis varied from a direction that was perpendicular to the MD at low stretch ratios to a direction that was parallel to the MD at high stretch ratios. Biangardi and Zachmann[41] studied the orientation distribution of amorphous PET film specimens, stretched uniaxially at 90°C to a stretch ratio of 4.4 at different stretch rates. They found that the higher the stretch

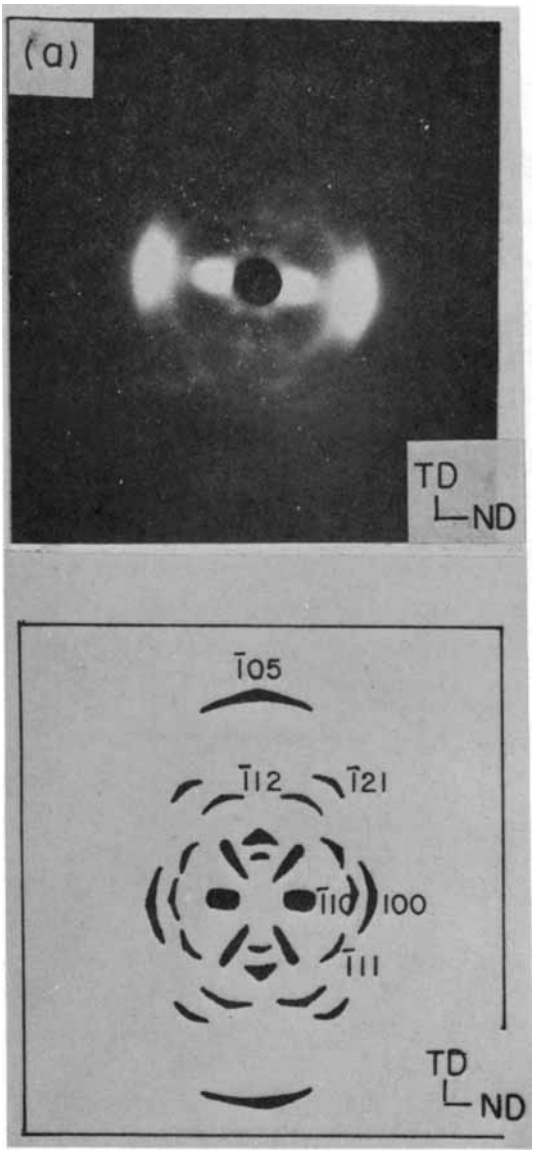

Fig. 10. The flat plate WAXS patterns of sample #7 taken with incident X-ray beam directed parallel to different directions: (a) MD; (b) TD; (c) ND.

rate, the greater the chain orientation. According to their results, the samples with low orientation had a fibrous structure with rotational symmetry about MD, but the samples with high orientation had a uniaxial planar orientation with (100) planes that were oriented parallel to the film surface. Misra and Stein[46] reported that, for amorphous PET film samples, stretched uniaxially at room temperature to a stretch ratio 2 at a stretch rate of 10% elongation per minute and annealed at 140°C for 10 min, the (010) and (100) reflection planes were located on the equator, indicating that these two planes were oriented parallel to the MD and that the *c*-axis was preferentially oriented parallel to the MD. It should be mentioned that none of the studies referred

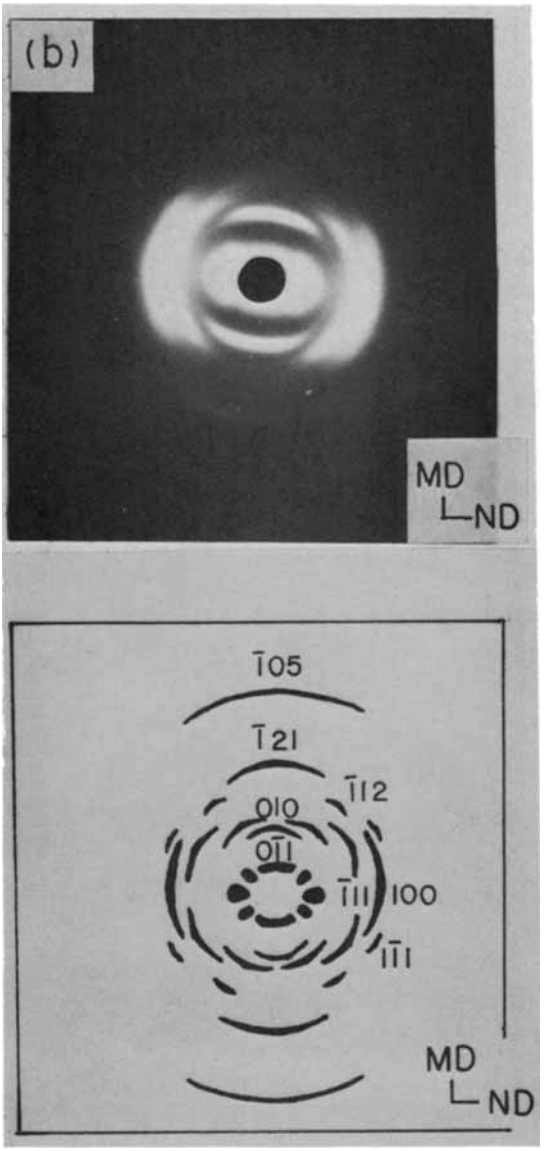

Fig. 10. (*Continued from the previous page.*)

to above used PET film samples that were biaxially oriented using a film blowing process.

Pole Figure Analysis

The pole figures of ($\bar{1}05$), (100), and (010) planes for samples #1 and #4 are given in Figures 11 and 12, respectively. Note that samples #1 and #4 have the same BUR 4.25, but the TUR of sample #1 is 38.7, while the TUR of sample #4 is 29.8. Figure 11 shows that in sample #1 the poles of ($\bar{1}05$) planes point to a direction that is between MD and TD. On the other hand, Figure 12 shows that in sample #4 the pole of the ($\bar{1}05$) planes point to a

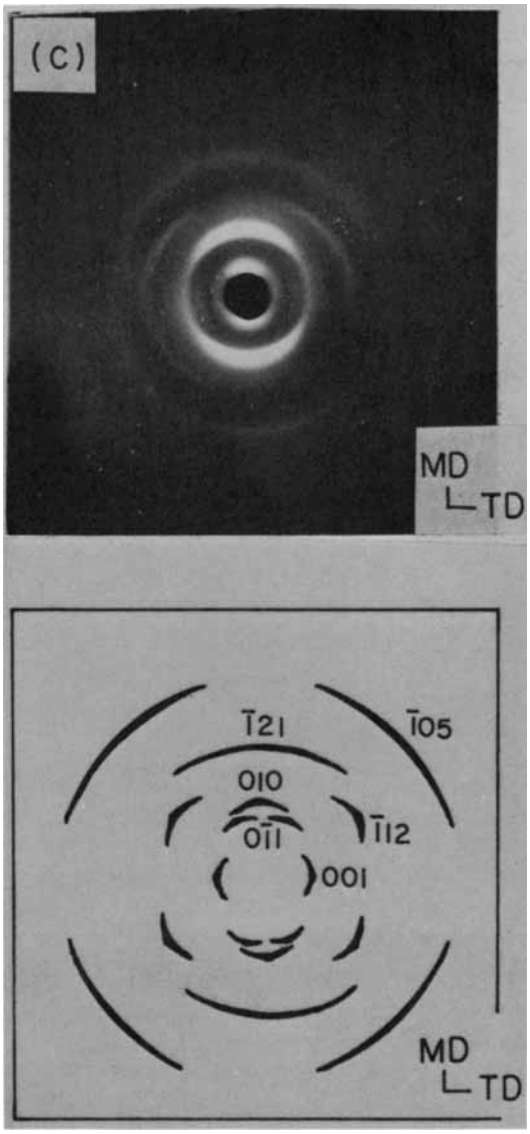

Fig. 10. *(Continued from the previous page.)*

direction that is nearly parallel to the TD. This observation is consistent with that made above with the flat plate patterns (see Figs. 7 and 8). Note in Figure 11 that the number of contour lines on the left-hand side is greater than that on the right-hand side of the (010) pole figure. There are two possibilities that might have contributed to the asymmetric pole figures observed. One is the asymmetricity in the shape of the blown bubble, i.e., during the film blowing operation, one side of the tubular bubble might have been blown up more than the opposite side, causing nonuniform molecular orientation in the film samples. The other possibility is that when preparing specimens for pole figure analysis by stacking together many layers of film samples, a perfect alignment might not have been realized. Since the film stack itself was not rigid enough

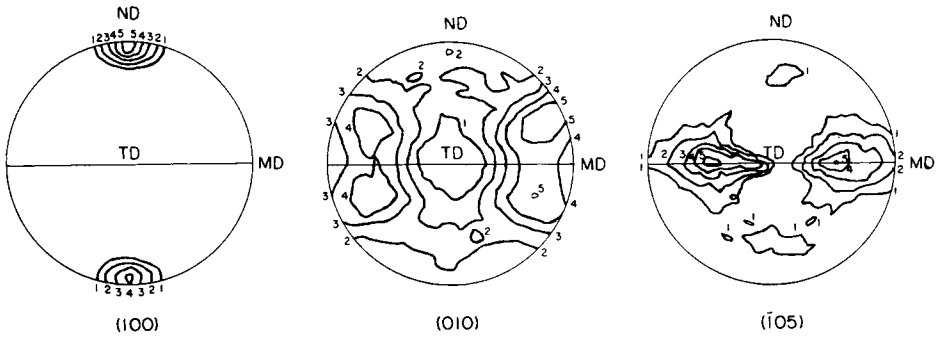

Fig. 11. Pole figures for sample #1 with TD as the spindle axis: (1) 3.8; (2) 5.0; (3) 6.3; (4) 7.5; (5) 8.8.

to be cut by a diamond saw, a razor blade was used to cut the film stack into the specified sample dimensions by hand, with the aid of a magnifying lens. If the hand-cut film stack was not symmetric, it would cause asymmetricity in the scattering volume. If the scattering volume was not symmetric, the scattered X-ray intensity could not be symmetric. Under such circumstances, a pole figure with asymmetric contour levels, such as the (010) pole figure in Figure 11, would be produced. It is believed that the latter possibility contributed more to the asymmetric (010) pole figures in Figure 11 than the former. Note in Figures 11 and 12 that the (100) poles are concentrated in the ND of the film. Since the (100) planes are nearly parallel to the benzene ring planes of the PET chains, Figures 11 and 12 indicate that the benzene ring planes are parallel to the film surface which is the equatorial plane of the pole figure. By comparing the (100) pole figure in Figure 11 with that in Figure 12, we observe in sample #4, which has a low TUR compared to sample #1, that the (100) poles are distributed more toward the MD of the sample, while the (010) poles point toward a direction between the TD and ND.

The pole figures of ($\bar{1}$05), (100), and (010) planes for samples #5 and #7 are given in Figures 13 and 14, respectively. Both samples have the same TUR 38.7, but sample #5 has a lower BUR than sample #7 (see Table I). It can be seen that the ($\bar{1}$05) poles in sample #5 point to the MD (see Fig. 13), while the ($\bar{1}$05) poles in sample #7 point to the TD (see Fig. 14). This suggests that as

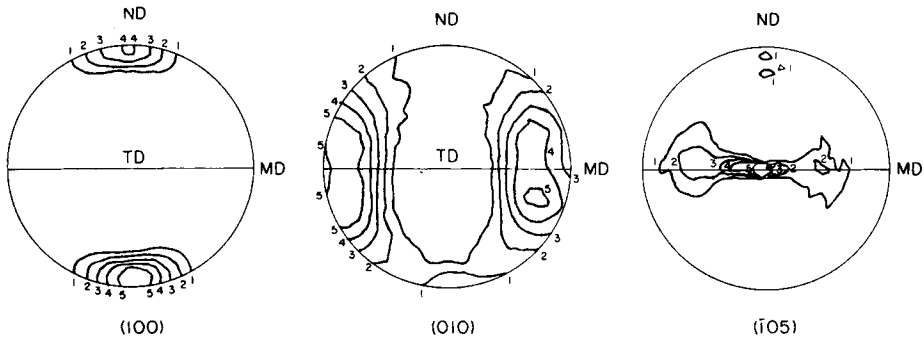

Fig. 12. Pole figures for sample #4 with TD as the spindle axis: (1) 3.8; (2) 5.0; (3) 6.3; (4) 7.5; (5) 8.8.

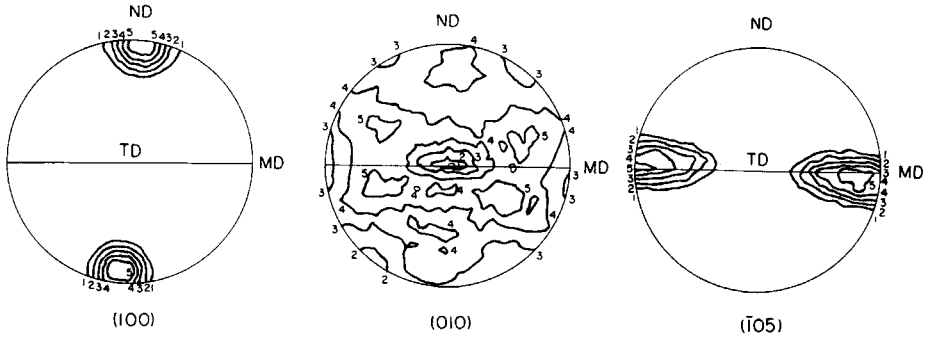

Fig. 13. Pole figures for sample #5 with TD as the spindle axis: (1) 3.8; (2) 5.0; (3) 6.3; (4) 7.5; (5) 8.8.

the BUR is increased, the (1̄05) poles are shifted from a direction pointing toward the MD to a direction pointing toward the TD of the specimens. The above observations are consistent with those made with the flat plate patterns (see Figs. 9 and 10). Note in Figures 13 and 14 that the (100) poles of samples #5 and #7 point toward the ND, indicating that the benzene ring planes of the PET chain molecules are parallel to the film surface. This confirms the results of the flat plate patterns [see Figs. 9(a), 9(b), 10(a), and 10(b)]. Although the difference in BUR between samples #5 and #7 is not large, it does seem to make some difference in the shape of the contours of the (100) pole figures, as observed in Figures 13 and 14. Note that the (010) poles point toward a direction that is between the MD and ND.

The crystalline orientation functions ($f_{i,j}$) of the (100), (010), and (1̄05) planes were calculated by substituting the corresponding second moments of orientation, $\langle \cos^2 \chi_{i,j} \rangle$, into eq. (4). Figure 15 gives the orientation triangle plot of $f_{1,j}$ vs. $f_{2,j}$ for the film samples investigated. It can be seen in Figure 15 that the values of the crystalline orientation functions of the (100) planes all fall closely in the lower left portion of the triangle. This implies that the (100) plane normal is parallel to the ND (3-axis) of the film. The data points are also located near the bisector of the angle $X_1X_3X_2$, suggesting that the (100) planes are nearly equibiaxially oriented. Except for sample #5, the values of $f_{i,j}$ of the (010) planes nearly all lie to the left of the ordinate. This

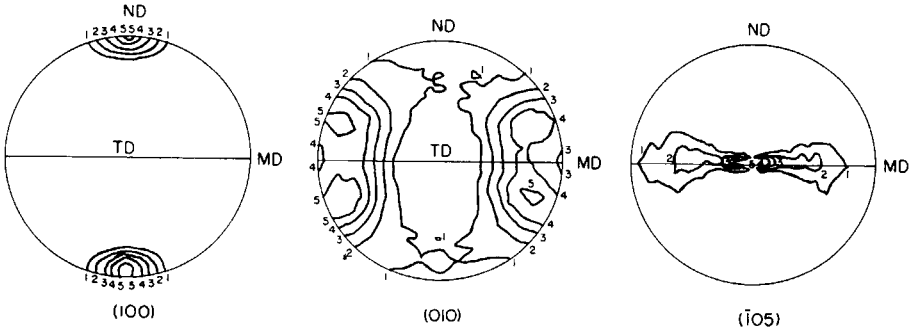

Fig. 14. Pole figures for sample #7 with TD as the spindle axis: (1) 3.8; (2) 5.0; (3) 6.3; (4) 7.5; (5) 8.8.

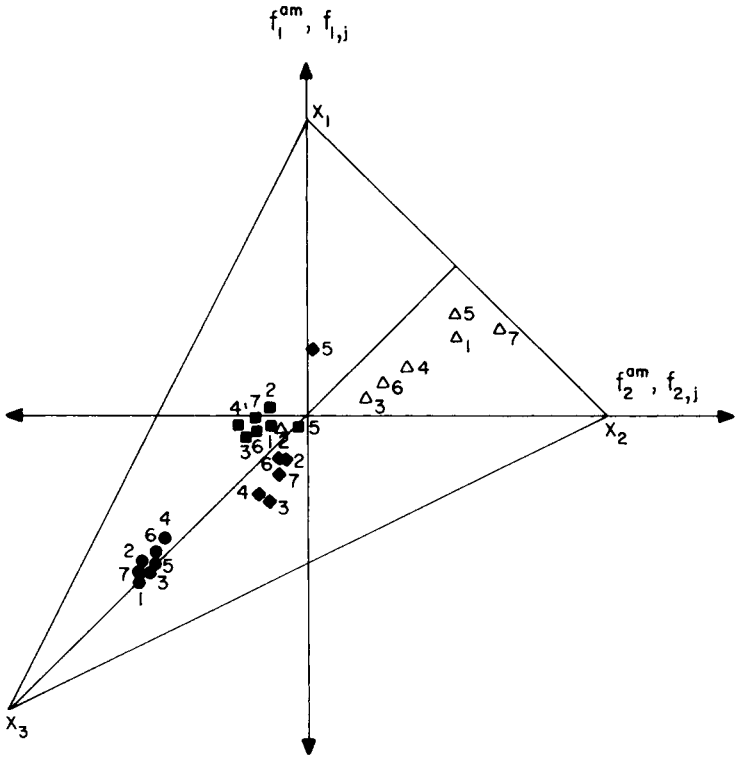

Fig. 15. The orientation triangle plot of $f_{1,j}$ vs. $f_{2,j}$: (●) (100) plane; (■) (010) plane; (◆) ($\bar{1}05$) plane. Also, f_1^{am} is plotted vs. f_2^{am} for amorphous orientation functions (Δ). The number for each symbol represents the sample identification number.

suggests that all the samples, except for sample #5, have their (010) poles pointed nearly perpendicular to the TD (2-axis) of the samples. Except for sample #5, the values $f_{i,j}$ of the ($\bar{1}05$) planes lie in the regions between the left of the ordinate and the bisector of angle $X_1X_3X_2$. This means that all the samples have their ($\bar{1}05$) poles, pointing toward a direction that is between the MD (1-axis) and TD (2-axis) of the film samples. The $f_{i,j}$ of the ($\bar{1}05$) planes for sample #5 indicate that the ($\bar{1}05$) poles are oriented uniaxially in the MD, and that the (010) poles point toward a direction which is parallel to the TD (2-axis) of the film sample.

The amorphous orientation functions, f_1^{am} and f_2^{am}, were also calculated by substituting the values of $f_{i,j}$, Δn_{13}, Δn_{23}, X, Δ_{cb}^{0cr}, Δ_{ab}^{0cr}, and Δ^{0am} into eq. (6), and neglecting the terms containing $\Delta n_{13,form}$ and $\Delta n_{23,form}$. In the calculations, the following values of the intrinsic birefringence, given by Yoshihara et al.,[43] were used: $\Delta_{cb}^{0cr} = 0.0326$, $\Delta_{ab}^{0cr} = -0.4040$, and $\Delta^{0am} = 0.2054$. Since the ($\bar{1}05$) and (100) plane normals are nearly parallel to the c- and a'-axes, respectively, the following assumptions were made in the calculations of f_i^{am}, i.e.,

$$\langle \cos^2 \chi_{i,c} \rangle = \langle \cos^2 \chi_{i,\bar{1}05} \rangle \tag{8a}$$

$$\langle \cos^2 \chi_{i,a'} \rangle = \langle \cos^2 \chi_{i,100} \rangle \tag{8b}$$

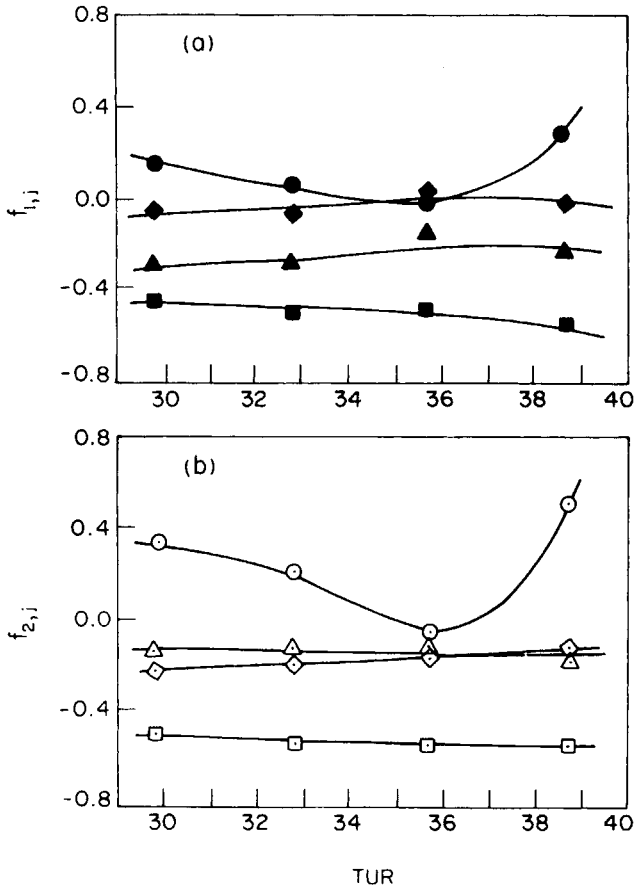

Fig. 16. (a) The effect of TUR on: (■) $f_{1,a}$; (◆) $f_{1,b}$; (▲) $f_{1,c}$; (●) f_1^{am} at a constant BUR 4.25. (b) The effect of TUR on: (⊡) $f_{2,a}$; (◇) $f_{2,b}$; (△) $f_{2,c}$; (⊙) f_2^{am} at a constant BUR 4.25.

Figure 15 gives a plot of f_1^{am} vs. f_2^{am}. It can be seen in Figure 15 that the chain axis of the amorphous phase is oriented more toward the TD (2-axis), than toward the MD (1-axis), except for sample #2. The chain axis of the amorphous phase for sample #2 is equibiaxially oriented between the MD (1-axis) and TD (2-axis), since the point representing its f_i^{am} lies near the bisector of the angle $X_1X_3X_2$.

The effects of TUR on $f_{i,j}$ and f_i^{am} for film samples with the same BUR are shown in Figure 16. It can be seen in Figure 16 that compared to f_i^{am}, the $f_{i,j}$ are relatively insensitive to TUR. The f_i^{am} were found to decrease with increasing TUR, until reaching a minimum at TUR = 35.7. It can be seen that a further increase in TUR would cause an increase in f_i^{am}. This can be attributed to the fact, at low TUR, the polymer chains are oriented more toward the TD than toward the MD. With an increase in TUR, more polymer chains become oriented toward the MD. A critical value of TUR, about 36, appears to exist, which changes the dependence of f_i^{am} on TUR.

The dependence of $f_{i,j}$ and f_i^{am} on BUR at a fixed value of TUR is given in Figure 17. It can be seen in Figure 17 that f_i^{am} is more sensitive to BUR than

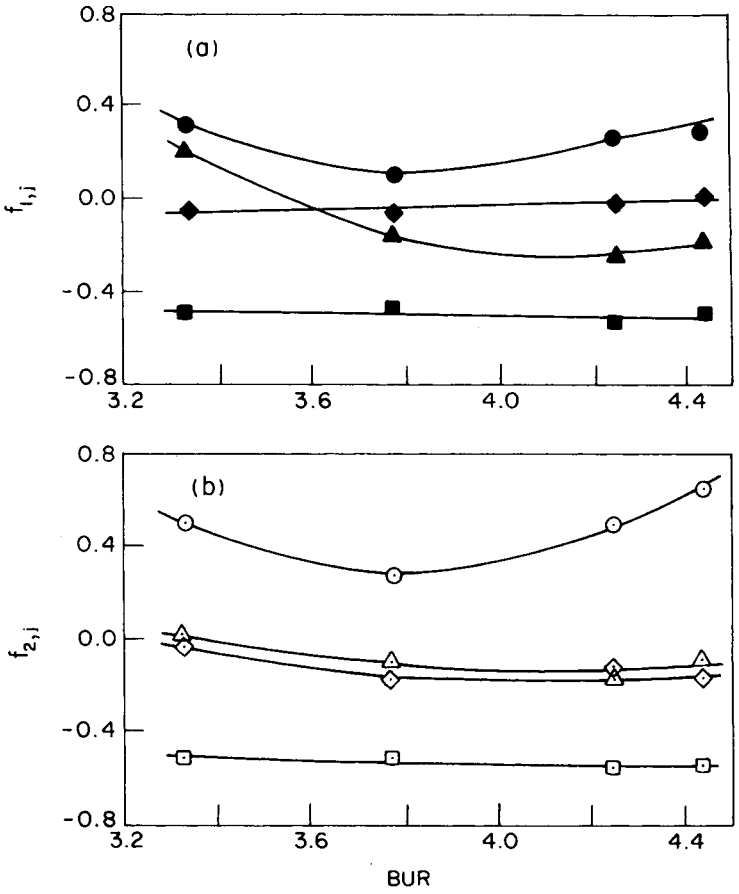

Fig. 17. (a) The effect of BUR on: (■) $f_{1,a}$; (◆) $f_{1,b}$; (▲) $f_{1,c}$; (●) f_1^{am}, at a constant TUR 38.7. (b) The effect of BUR on (⊡) $f_{2,a}$; (◇) $f_{2,b}$; (△) $f_{2,c}$; (⊙) f_2^{am} at a constant TUR 38.7.

$f_{i,j}$, and that f_i^{am} goes through a minimum with increasing BUR. Again, a critical value of BUR appears to exist, which changes the dependence of f_i^{am} on BUR. This is attributable to the fact that the polymer chains tend to be oriented toward the MD at small BUR, and, as the BUR is increased, the polymer chains become more oriented toward the TD.

It would be appropriate to mention, at this juncture, some of the earlier investigations that are relevant to the results presented above. Heffelfinger and Burton[47] reported that the (100) planes were found to be parallel with the film surface for biaxially oriented PET film samples. DeVries et al.[37] reported that the fraction of randomly oriented (100) planes in biaxially oriented PET film specimens decreased with increasing stretch ratio. Yoshihara et al.[43] observed preferential uniplanar orientation of the benzene ring planes to the film surface for biaxially stretched PET films. Sakaguchi et al.[48] noted that uniplanar orientation of the (100) planes and planar orientation of the *c*-axis were developed during biaxial stretching of PET film, where the extent of the orientation was found to be dependent upon the stretch ratio and the mode of biaxial stretching. Cakmak et al.[49] reported that for PET film samples that

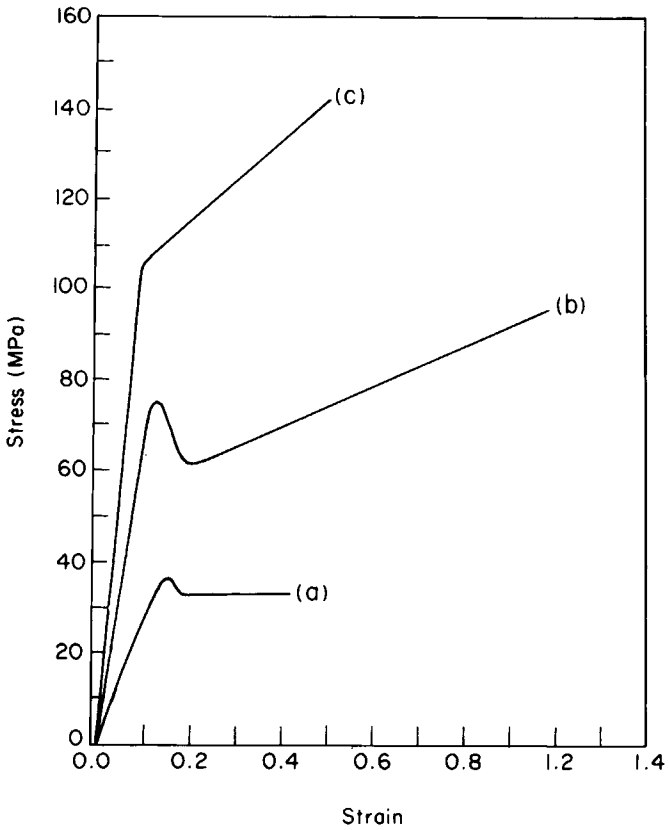

Fig. 18. Stress–strain curves for PET blown film samples: (a) unoriented sample; (b) sample stretched at 83°C; (c) sample stretched at 83°C and annealed at 200°C for 220 s.

had been equibiaxially stretched at 80–100°C, the *c*-axis was oriented equibiaxially and the benzene ring plane was oriented parallel to the film surface. It should be pointed out that none of the studies referred to above employed samples that had been prepared using a film blowing process.

Effects of Processing Conditions on Tensile Mechanical Properties

Figure 18 gives stress-strain curves for an unoriented blown film specimen, and for both annealed and unannealed PET film specimens that were stretched at 83°C. It can be seen in Figure 18 that among the three samples, the annealed film sample stretched at 83°C had the largest tensile stress-at-break (σ_B).

The effect of stretch temperature (T_s) on the σ_B of the annealed samples, as functions of TUR and BUR, are shown in Figures 19 and 20, respectively. It can be seen in Figures 19 and 20 that the samples stretched at 83°C have higher σ_B than those stretched at 90°C. This can be attributed to the fact that a film stretched at a low temperature retains a higher level of orientation than one stretched at a higher temperature, since the lower the T_s, the more

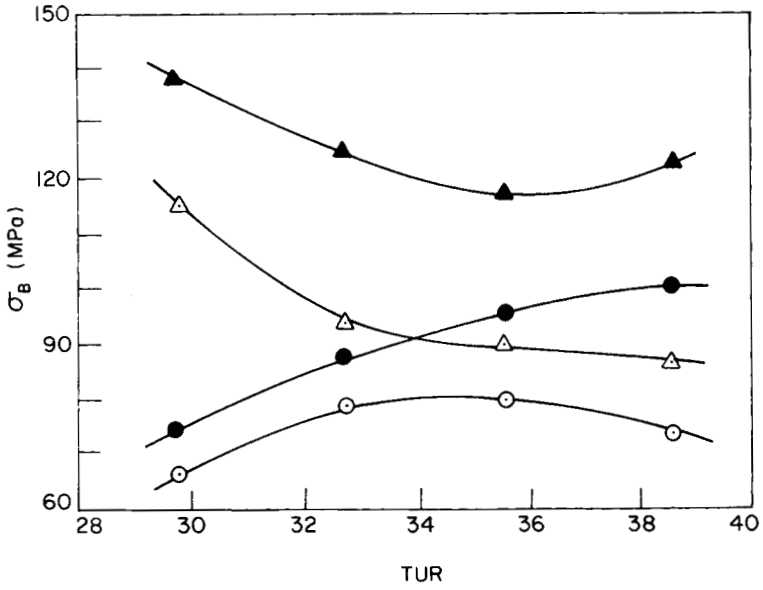

Fig. 19. The effect of TUR on σ_B for samples at a constant BUR 4.25 and annealed at 200°C for 220 s. (a) Samples stretched at 83°C: (●) σ_B in the MD; (▲) σ_B in the TD. (b) Samples stretched at 90°C: (⊙) σ_B in the MD; (△) σ_B in the TD.

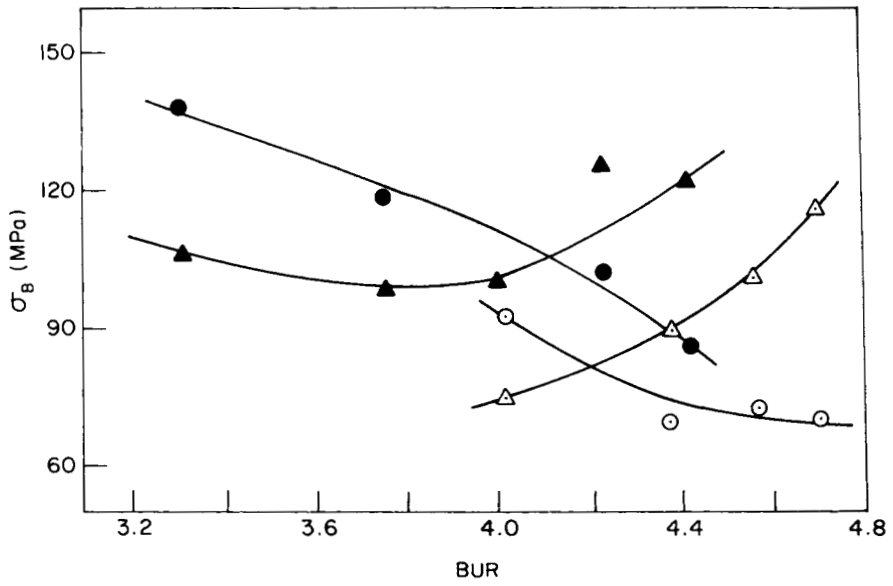

Fig. 20. The effect of BUR on σ_B for samples at a constant TUR 38.7 and annealed at 200°C for 220 s. (a) Samples stretched at 83°C: (●) σ_B in the MD; (▲) σ_B in the TD. (b) Samples stretched at 90°C: (⊙) σ_B in the MD; (△) σ_B in the TD.

difficult it becomes for the oriented chains to relax during film blowing. Therefore, it can be concluded from Figures 19 and 20 that the large values of σ_B observed in the film samples stretched at 83°C, compared to the samples stretched at 90°C, are attributable to greater chain orientation in the samples. Judging from the differences in σ_B observed in Figures 19 and 20, the stretch temperature appears to be one of the most important processing variables which greatly affect σ_B. A close examination of Figures 16 and 19 reveals that σ_B in the TD is greatly influenced by the amorphous orientation functions f_i^{am}, while the σ_B in the MD is not. It can also be seen in Figures 17 and 20 that σ_B in the TD is greatly influenced by f_i^{am}, while σ_B in the MD is not. In other words, we can see a clear correlation between the amorphous orientation functions and the tensile mechanical properties of PET blown film samples.

The effect of TUR on tensile modulus for the annealed film samples, stretched at 83°C and at a constant BUR of 4.25, is shown in Figure 21. It can be seen in Figure 21 that the tensile modulus in the MD increased, while the tensile modulus in the TD decreased, with increasing TUR. At present, we cannot explain why data points at the TUR value of about 35.7 deviate considerably from the observed correlation. According to the results of the pole figure analyses given in Figures 11 and 12, at low TUR, the polymer chains are highly oriented in a direction that is parallel to the TD, while at high TUR the polymer chains are oriented toward a direction that is somewhere between the TD and MD. This can explain why at low TUR, the tensile modulus in the TD is higher than that in the MD, and why the differences in the tensile modulus between the MD and TD become smaller as the TUR is increased.

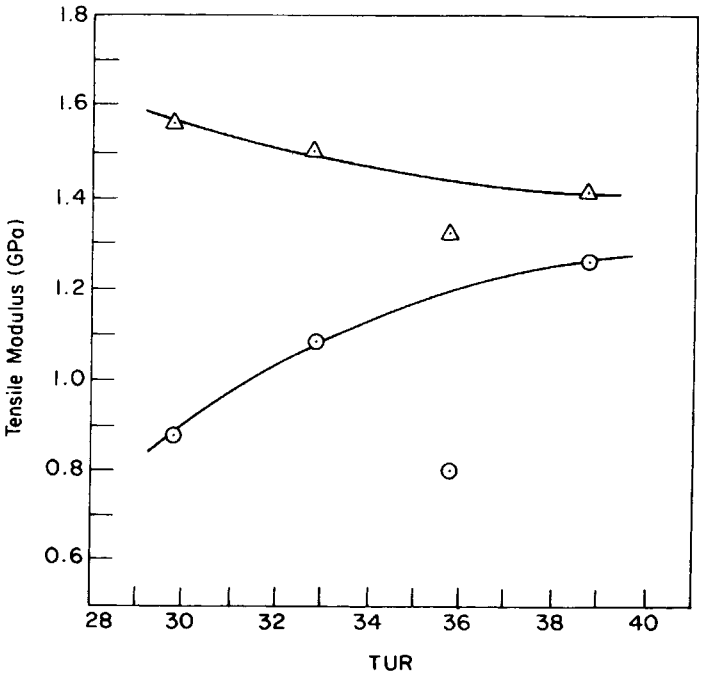

Fig. 21. The effect of TUR on tensile modulus for samples stretched at 83°C at a constant BUR 4.25: (⊙) tensile modulus in the MD; (△) tensile modulus in the TD.

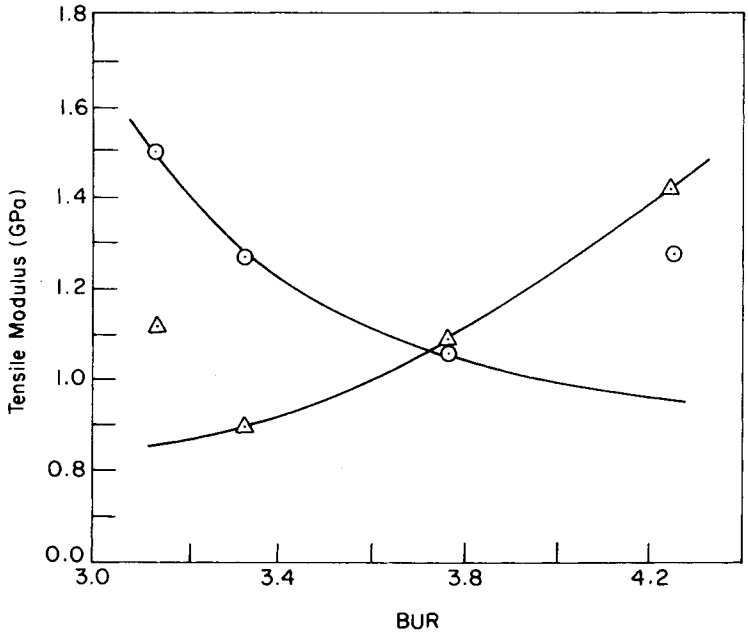

Fig. 22. The effect of BUR on tensile modulus for samples stretched at 83°C at a constant TUR 38.7: (⊙) tensile modulus in the MD; (△) tensile modulus in the TD.

The effect of BUR on the tensile modulus for the annealed film samples, stretched at 83°C and at a constant TUR of 38.7, is shown in Figure 22. It can be seen in Figure 22 that the tensile modulus in the TD increased, while the tensile modulus in the MD decreased, with increasing BUR. The pole figures given in Figures 13 and 14 indicate that, at low BUR, the polymer chains are aligned parallel to the MD, while at high BUR the polymer chains are oriented in a direction that is parallel to the TD. Therefore, it would be reasonable to expect that, at low BUR, the tensile modulus would be greater in the MD than in the TD, and, at high BUR, the tensile modulus would be greater in the TD than in the MD.

CONCLUDING REMARKS

From the bulk birefringence measurements, the following conclusions may be drawn: (1) The magnitude of Δn_{13} and Δn_{23} for the PET blown film samples are influenced by the stretch temperature, takeup ratio, and blowup ratio; (2) by annealing, under constraint at 200°C for 220 s, the PET blown film samples that had been stretched at 83°C, the birefringence of the samples increased considerably, compared to the unannealed ones, owing to an improvement in both the degree of crystallinity and the structural perfection during annealing. From the density measurements, we have found that annealing of PET blown films under constraint significantly increased the degree of crystallinity, indicating that the structural ordering was improved during annealing.

From the WAXS flat plate patterns, we have found that the benzene ring planes of the annealed samples were aligned in a direction parallel to the film surface and that chain orientation in the PET blown film was quite sensitive

to the processing variables. Specifically, we have observed that: (1) for samples with a BUR 4.25–4.44 and a TUR 38.7, the polymer chains were oriented in a direction which is closer to the TD than to the MD; (2) for the sample with a BUR 4.25 and a TUR 29.8, the polymer chains aligned in a direction that is nearly parallel to the TD; and (3) for the sample with a BUR 3.33 and a TUR 38.7, the polymer chain axis aligned in a direction that is nearly parallel to the MD. The above results from the WAXS flat plate patterns were confirmed by pole figure analysis. Pole figure analysis has revealed further that the crystalline orientation functions are relatively insensitive to stretch ratios (i.e., TUR and BUR) for the PET blown film samples, stretched at 83°C and subsequently annealed under constraint at 200°C for 220 s.

From the measurements of tensile mechanical properties, the following conclusions may be drawn: (1) it is possible to fabricate equibiaxially oriented PET films via a film blowing process; (2) the σ_B of equibiaxially oriented PET blown film samples increases with decreasing stretch temperature and increasing annealing temperature; and (3) the deformation and thermal histories of PET blown film samples have significant effects on their mechanical properties.

It was observed that σ_B in the TD is greatly influenced by the amorphous orientation functions f_i^{am}, while the σ_B in the MD is not. It was concluded from the present investigation that equibiaxially oriented PET blown films with high tensile strength can be produced by judiciously selecting an optimum processing condition.

The authors wish to acknowledge with deep gratitude that Dr. Tae Hoon Kwack at Mobil Chemical Company arranged for us to use a birefringence apparatus and that Professor Mukerrem Cakmak helped us to take the pole figures reported in this paper, using the facilities at the Polymer Engineering Center at the University of Akron. Without the generous help received from them, the completion of this study would not have been possible.

References

1. C. J. Heffelfinger and K. L. Knox, in *The Science and Technology of Polymer Films*, O. J. Sweeting, Ed., Wiley-Interscience, New York, 1971, Vol. 2, Chap. 4.
2. J. H. Briston and L. L. Katan, *Plastics Films*, 2nd ed., Longman, New York, 1983.
3. R. S. Stein, in *Newer Methods of Polymer Characterization*, B. Ke, Ed., Wiley-Interscience, New York, 1964, Chap. 4.
4. L. E. Alexander, *X-Ray Diffraction Methods in Polymer Science*, Wiley, New York, 1969, Chap. 4.
5. J. F. Rabek, *Experimental Methods in Polymer Chemistry*, Wiley, New York, 1980.
6. R. J. Samuels, *Structured Polymer Properties*, Wiley, New York, 1974.
7. I. M. Ward, Ed., *Structure and Properties of Oriented Polymer*, Wiley, New York, 1975.
8. J. R. A. Pearson and C. J. S. Petrie, *J. Fluid Mech.*, **40**, 1 (1970).
9. C. D. Han and J. Y. Park, *J. Appl. Polym. Sci.*, **19**, 3277 (1975).
10. J. Haw and C. D. Han, 20th ANTEC Preprint, SPE, 1984, p. 181.
11. P. L. Clegg and N. D. Huck, *Plastics (London)*, **26**, 114 (1961).
12. E. S. Clark and C. A. Garber, *Int. J. Polym. Mater.*, **1**, 31 (1971).
13. D. R. Holmes and R. P. Palmer, *J. Polym. Sci.*, **31**, 345 (1958).
14. S. L. Aggarwal, G. P. Tilley, and O. J. Sweeting, *J. Appl. Polym. Sci.*, **1**, 91 (1959).
15. P. H. Lindenmeyer and S. Lustig, *J. Appl. Polym. Sci.*, **9**, 227 (1965).
16. C. R. Desper, *J. Appl. Polym. Sci.*, **13**, 169 (1969).
17. T. Nagasawa, T. Matsumura, and S. Hoshino, *Appl. Polym. Symp.*, **20**, 295 (1973).

18. W. F. Maddams and J. E. Preedy, *J. Appl. Polym. Sci.*, **22**, 2721 (1978).
19. K. J. Choi, J. E. Spruiell, and J. L. White, *J. Polym. Sci., Polym. Phys., Ed.*, **20**, 27 (1982).
20. W. F. Maddams and M. E. Vickers, *J. Elast. Plast.*, **15**, 246 (1983).
21. H. Ashizawa, J. E. Spruiell, and J. L. White, *Polym. Eng. Sci.*, **24**, 1035 (1984).
22. A. J. DeVries, *Pure Appl. Chem.*, **53**, 1011 (1981).
23. Y. Shimomura, J. E. Spruiell, and J. L. White, *J. Appl. Polym. Sci.*, **27**, 2663 (1982).
24. M. F. Bottin, M. Boudeulle, and J. Guillet, *J. Polym. Sci., Polym. Phys.*, **21**, 401 (1983).
25. K. J. Choi, J. L. White, and J. E. Spruiell, *J. Appl. Polym. Sci.*, **25**, 2777 (1980).
26. K. Matsumoto, J. F. Fellers and J. L. White, *J. Appl. Polym. Sci.*, **26**, 85 (1981).
27. R. S. Stein, *J. Polym. Sci.*, **24**, 383 (1957).
28. R. D. Daubeny, C. W. Bunn, and C. J. Brown, *Proc. Roy. Soc.*, **226A**, 531 (1954).
29. J. J. Hermans, P. H. Hermans, D. Vermaas, and A. Weidinger, *Rec. Trav. Chim.*, **65**, 427 (1946).
30. R. S. Stein, *J. Polym. Sci.*, **21**, 381 (1956).
31. Z. W. Wilchinsky, in *Advances in X-Ray Analysis*, W. M. Mueller and M. Fay, Eds., Plenum, New York, 1962, Vol. 6, p. 231.
32. J. L. White and J. E. Spruiell, *Polym. Eng. Sci.*, **21**, 859 (1981).
33. Z. W. Wilchinsky, *J. Appl. Phys.*, **30**, 792 (1959).
34. G. L. Wilkes, *J. Macromol. Sci., Rev. Macromol. Chem.*, **C10(2)**, 149 (1974).
35. J. L. White and J. E. Spruiell, *Polym. Eng. Sci.*, **23**, 247 (1983).
36. T. C. Furnas and D. Harker, *Rev. Sci. Instr.*, **26**, 449 (1955).
37. A. J. DeVries, C. Bonnebat, and J. Beautemps, *J. Polym. Sci., Symp.*, **58**, 109 (1977).
38. S. A. Jabarin, *Polym. Eng. Sci.*, **24**, 378 (1984).
39. M. Cakmak, J. E. Spruiell, and J. L. White, *Polym. Eng. Sci.*, **24**, 1390 (1984).
40. M. Yokouchi, Y. Hiromoto, and Y. Kobayashi, *J. Appl. Polym. Sci.*, **24**, 1965 (1979).
41. H. J. Biangardi and H. G. Zachmann, *J. Polym. Sci. Symp.*, **58**, 169 (1977).
42. H. G. Zachmann, *Polym. Eng. Sci.*, **19**, 966 (1979).
43. N. Yoshihara, A. Fukushima, Y. Watanabe, A. Nakai, S. Nomura, and H. Kawai, *Sen-I Gakkaishi*, **37**, T-387 (1981).
44. T. C. Ma, Ph.D. Dissertation, Polytechnic University, Brooklyn, New York, 1987.
45. W. J. Dulmage and A. L. Geddes, *J. Polym. Sci.*, **31**, 499 (1958).
46. A. Misra and R. S. Stein, *J. Polym. Sci. Polym. Phys.*, **17**, 235 (1979).
47. C. J. Heffelfinger and R. L. Burton, *J. Polym. Sci.*, **47**, 289 (1960).
48. N. Sakaguchi, T. Oda, A. Nakai, and H. Kawai, *Sen-I Gakkaishi*, **33**, T-499 (1977).
49. M. Cakmak, J. L. White, and J. E. Spruiell, *J. Polym. Eng.*, **6**, 291 (1986).

Received May 19, 1987
Accepted July 27, 1987